

Structural stabilities, elastic constants, generalized stacking fault energetics, and the martensitic transformation mechanisms for the $\text{Ni}_{50-x}\text{TiPt}_x$ ($x = 0 - 30$) ternary system: *ab initio* investigation

N. Hatcher^{1,a}, O. Yu. Kontsevoi¹, and A. J. Freeman^{1,2}

¹ Department of Physics and Astronomy, Northwestern University, Evanston, Illinois 60208, USA

² Department of Materials Science and Engineering, Northwestern University, Evanston, Illinois 60208, USA

Abstract. To determine the effect of ternary additions on the martensitic behavior of NiTi, we apply *ab initio* calculations using the highly precise full-potential linearized augmented plane wave method to the Ni-Ti-Pt system. We compare formation energies of various stoichiometries and the pair energetics between Pt atoms to create a number of model austenite structures, finding that Pt atoms prefer to decorate the lattice at third nearest neighbors from one another, and establish the hierarchy among the austenitic and martensitic phases. We examine the structural stability to determine the susceptibility toward displacive phase transformation: namely, we calculate planar generalized stacking fault energetics of major shear planes including the {100}, {011}, and {111} planes and we calculate and compare the elastic constants of each phase. We show that increased Pt content causes a dramatic softening of the austenite C' elastic constant and increased rigidity in the martensite, and there is a high resistance to {100} shear similar to equiatomic NiTi. Finally, we explore a martensitic mechanism of this alloy and explain how the transformation path and energy barriers of the NiTi system are affected by Pt.

1 Introduction

The novel properties of nickel-titanium based shape memory alloys have been exploited to create numerous devices that utilize the thermo/piezo mechanical coupling. These alloys are biocompatible, inexpensive, and have good dimensional stability, giving them potential use in a wide range of applications. However, for high temperature applications, such as components of jet engines, the martensitic transformation temperature in near equiatomic NiTi is too low to be usefully employed as novel actuation systems. Thus, there is an ongoing search for materials that can raise the martensitic transformation temperature of this system without losing dimensional stability and work output.

Additions of Pt to the nickel-titanium system have been shown to raise the martensitic finish temperature from near room temperature to above 200°C and higher [1]. We study this system using first-principles density functional theory calculations to determine how Pt substitutions affect the martensitic transformation by examining changes in crystal structures,

^a e-mail: n-hatcher@northwestern.edu

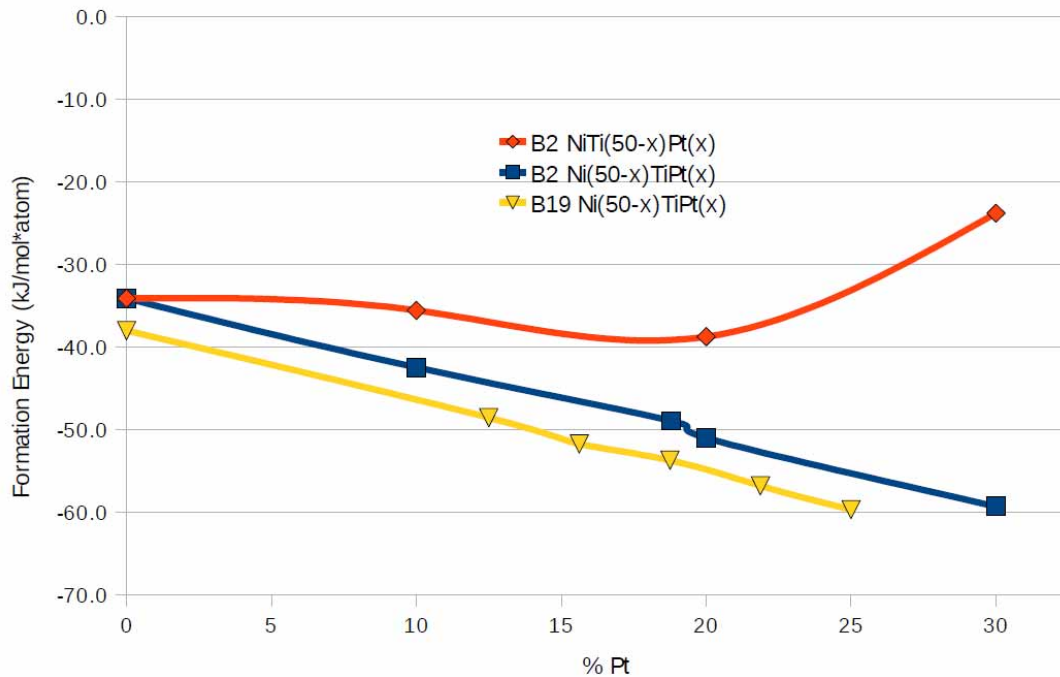


Fig. 1. The formation energies of the relaxed $N_{50-x}Ti_{50}Pt_x$ and $Ni_{50}Ti_{50-x}Pt_x$ B2 and $Ni_{50-x}Ti_{50}Pt_x$ B19 structures versus Pt concentration ($x = 0 - 30$).

site occupation, elastic properties, shear energetics, and changes to the electronic structure. A more complete understanding of the fundamental properties will reduce the need for expensive and time consuming alloy preparation, characterization, and testing. Additionally, these *ab initio* results may be used as input parameters for higher order modeling, e.g. phase field and micromechanical approaches.

2 Computational Details

Density functional electronic structure calculations were performed using the highly precise full-potential linearized augmented plane wave (FLAPW) method [2]. This method uses no shape approximations for the potential and charge density. The exchange correlation contribution to the potential was included using the generalized gradient approximation (GGA) within the Perdew-Burke-Ernzerhof functional [3] for all calculations. The plane wave cutoff was set to 275 eV, and the cutoff of the potential representation was set to 1,360 eV. A k-point mesh of $13 \times 13 \times 13$ was employed for all calculations which satisfied total energy convergence to within 1.5 meV/atom for the B2 structure and 0.4 meV/atom in each of the other structures. The muffin tin radii of Ti and Ni atoms were taken to be 2.35, 2.40, and 2.10 a.u., respectively. For a more accurate treatment of extended core electrons (i.e. Ti 3*p* electrons) that are not entirely contained within muffin tin spheres (also known as semi-core states), and which break the orthogonality between core and valence states, the method of explicit orthogonalization (XO) was used [4]. Supercells were constructed and relaxed targeting various concentrations of the ternary element, Pt. Methods for the calculation of elastic constants are explain in Ref. [5].

2.1 Results and Discussion

Numerous first-principles calculations have been performed on NiTi [5–10], but there have been relatively few attempts to understand ternary additions to this system [11,12]. A thorough

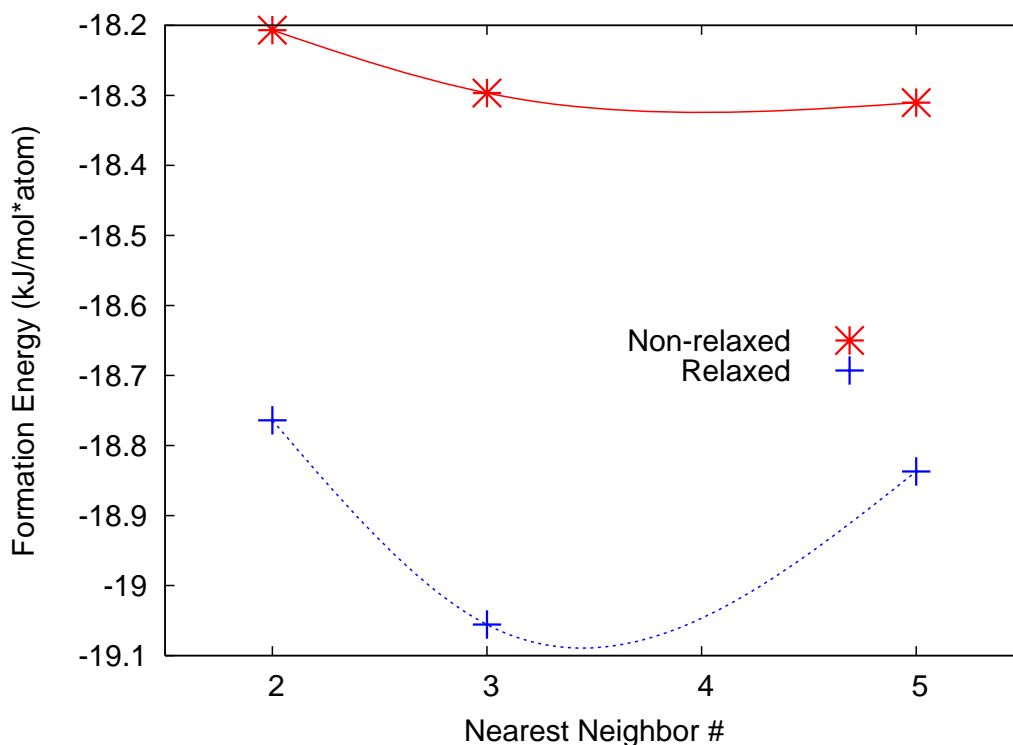


Fig. 2. Pair energetics of Pt atoms in the $\text{Ni}_{46.3}\text{Ti}_{50}\text{Pt}_{3.7}$ $3 \times 3 \times 3$ B2 supercell for relaxed and non-relaxed atomic positions.

investigation of ternary alloys involves finding the site preferences of the constituents, pair interaction energies between solute atoms, and atomic reorganization arising from these effects.

Formation energies explain solubility and indicate preferential structures and stoichiometries in materials. To determine these properties of the Ni-Ti-Pt system, we constructed $2 \times 2 \times 2$ supercells of the B2 structure, and calculated the formation energy for several compositions of Pt replacing Ni or Ti sites (see Fig. 1). The formation energy of $\text{Ni}_{50-x}\text{Ti}_{50}\text{Pt}_x$ decreases monotonically with increasing x , while the formation energy of $\text{Ni}_{50}\text{Ti}_{50-x}\text{Pt}_x$ is roughly flat, decreases at $x=20$, and then increases at higher x values. As lower formation energies are preferred, it is favorable for Pt atoms to replace Ni atoms. Also, given the monotonic decrease in formation energy for B2 $\text{Ni}_{50-x}\text{Ti}_{50}\text{Pt}_x$, Pt has high solubility in NiTi and its concentration may be varied to create desired properties, i.e. tune the martensitic finish temperature without Pt segregation.

Focusing on the $\text{Ni}_{50-x}\text{Ti}_{50}\text{Pt}_x$ system, we determine the Pt site preference by first calculating the pair energies of Pt in NiTi. This is accomplished by calculating the total energies with and without atomic relaxation of a $3 \times 3 \times 3$ B2 NiTi supercell with two Pt atoms substituting Ni atoms ($x=3.7$) at various nearest neighbor (NN) distances from one another. For the non-relaxed case, the third and fifth nearest neighbor (NN) sites have nearly equal formation energies and are slightly preferred (≈ 0.1 kJ/mol*atom) to the second NN sites (see Fig. 2). When atomic relaxation is employed, the formation energy of the third NN pairing is lowered below that of the fifth NN pairing. While small, this ordering is preferred due to relaxation effects which may be summarized as follows: relaxation of the third NN structure causes all surrounding atoms to relax away from the Pt pair. However, for the fifth NN case, a titanium atom sits directly between the two Pt atoms. This restricts the system's ability to relax fully. Thus, platinum atoms will prefer to order as third nearest neighbors.

Ab initio calculations have been known to predict accurate structural parameters of metals including NiTi [7–10]. Here, we calculate the structural parameters of $\text{Ni}_{50-x}\text{Ti}_{50}\text{Pt}_x$. The

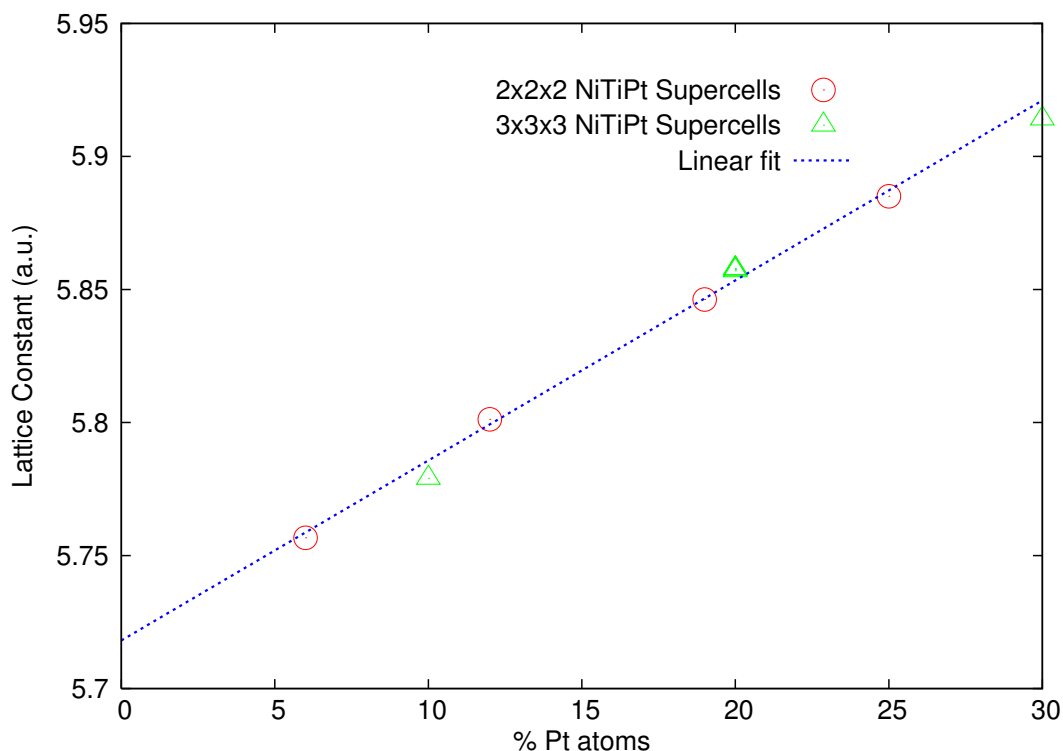


Fig. 3. Lattice constant of $\text{Ni}_{50-x}\text{Ti}_{50}\text{Pt}_x$ as a function of Pt concentration in B2 supercells.

lattice constant of the B2 structure was calculated with $2 \times 2 \times 2$ and $3 \times 3 \times 3$ supercells over a range of x values from 0 to 30. We observe a linear fit between the lattice constant and x with a y -intercept of 3.026 \AA (see Fig. 3), a 0.4% elongation from experiment. Neutron diffraction data gives a lattice constant of $a = 3.087 \text{ \AA}$ for the $\text{Ni}_{39}\text{Ti}_{50}\text{Pt}_{21}$ system [13] versus a calculated value of 3.101 \AA , a 0.4% difference. Since the GGA exchange correlation potential often slightly overestimates lattice constants, this represents strong agreement with experiment.

For the martensitic B19 structure, we calculated a , b , and c lattice constants to be 4.739 \AA , 2.867 \AA , and 4.302 \AA compared to experimental values of 4.672 \AA , 2.774 \AA , and 4.447 \AA resulting in errors of 1.4%, 3.2%, and -3.4%, respectively. While the volume differs by only 1.4%, the differences in the a and c lattice constants are likely due to the random Pt ordering as there may be multiple metastable coexisting phases arising from the Pt ordering in the austenite. Thus, several martensitic structures with slightly different lattice parameters and atomic coordinates may appear due to single crystal structural differences in the martensitic variants.

In NiTi the formation energy difference between the martensite, B19', and the austenite, B2, is 5.8 kJ/mol*atom [5]. Interestingly, the formation energy differences between the martensite of $\text{Ni}_{50-x}\text{Ti}_{50}\text{Pt}_x$ and its austenite remain constant for most values of x , around 4.5 to 6 kJ/mol*atom (see Fig. 1). Thus, the energy differences driving the martensitic transformation remains constant for various concentrations of Pt.

Single crystal and extrapolated polycrystalline elastic constants predict material properties including ductility, hardness, plastic response to deformation, and precursory indicators of instabilities to martensitic transformation. The single crystal and Hill averaged [14] (the average of Voigt [15] and Reuss [16] approximations to the elastic moduli) moduli are presented in Table 1. For the $\text{Ni}_{50-x}\text{Ti}_{50}\text{Pt}_x$ system, we investigated the effects of increasing x from 0 to 25. We found that C_{12} increases with Pt concentration while simultaneously decreasing C' , which, in turn, shows a precursory instability to B19 formation. Additionally, C_{44} increases with Pt concentration which serves to restrict any angle relaxation of the system, acting as a barrier to monoclinic B19' structure formation. Once the transformation has occurred, the stability of the

Table 1. Elastic constants of NiTiPt (GPa)

Structure	B2					B19
	NiTi	Ni ₄₄ Ti ₅₀ Pt ₆	Ni ₃₈ Ti ₅₀ Pt ₁₂	Ni ₃₁ Ti ₅₀ Pt ₁₉	Ni ₂₅ Ti ₅₀ Pt ₂₅	Ni ₃₁ Ti ₅₀ Pt ₁₉
C_{11}	183	169	170	167	178	242
C_{12}	146	155	161	168	184	163
C_{44}	46	49	53	53	57	51
B	159	161	164	166	169	156
C'	18.5	6.8	4.4	-0.2	-3.1	24.8
A	2.49	7.18	12.06	N/A	N/A	2.06
$A^{-1/2}$	0.63	0.37	0.29	N/A	N/A	0.70
G	32	23	22	15	12	47
ν	0.41	0.43	0.44	0.46	0.47	0.38
G/B	0.20	0.14	0.13	0.09	0.07	0.27
E	90	66	62	43	34	129

Table 2. GSF energy barriers and unstable stacking fault energies for NiTi and NiTiPt. Brackets ([]) denote the energy barrier along the Burger's vector that do not occur at the unstable stacking fault. For the 2 layer (011) case, relaxation was employed and the relaxed energy barriers are shown in parenthesis.

Plane	# Layers	NiTi		NiTiPt	
		Barrier Direction	Barrier (J/m ²)	Barrier Direction	Barrier (J/m ²)
(001)	2	$\langle 100 \rangle$ or $\langle 010 \rangle$	4.17	$\langle 100 \rangle$ or $\langle 010 \rangle$	4.02
	3	$\langle 100 \rangle$ or $\langle 010 \rangle$	4.20	$\langle 100 \rangle$ or $\langle 010 \rangle$	2.98
	4	$\langle 100 \rangle$ or $\langle 010 \rangle$	4.28	$\langle 100 \rangle$ or $\langle 010 \rangle$	3.62
	6	$\langle 100 \rangle$ or $\langle 010 \rangle$	4.30	$\langle 100 \rangle$ or $\langle 010 \rangle$	2.92
(011)	1	$\langle 111 \rangle$	1.79	$\langle 111 \rangle$	0.72[1.58]
	2	$\langle 111 \rangle$ ($\langle 100 \rangle$)	1.39 (0.31)	$\langle 111 \rangle$ ($\langle 100 \rangle$)	0.34[0.93] (0.17)
	3	$\langle 111 \rangle$	1.26	$\langle 111 \rangle$	0.97[1.64]
	4	$\langle 111 \rangle$	0.89	$\langle 111 \rangle$	0.66
	6	$\langle 111 \rangle$	1.06	$\langle 111 \rangle$	0.61

system is regained as C' of the B19 structure is positive and higher than that of the binary B2 system. Additionally, C_{11} for the Ni₃₁Ti₅₀Pt₁₉ B19 structure is approximately 60 GPa higher than each of the B2 structures indicating a harder phase.

To further examine ductility, hardness, and plasticity, we compare changes in the anisotropy factor ($A^{-1/2}$), the shear (G), bulk (B), and Young's (E) moduli, and the Poisson ratio (ν) across various stoichiometries and phases (see Table 1). The shear modulus decreases with increased Pt, which leads to a slight G/B decrease. Pugh [17] proposed an empirical criterion which requires that G/B is less than 0.57 for ductile metals. This is met for each of the structures and stoichiometries studied. A second criterion for ductility in metals is that the anisotropy factor is greater than 0.8 and Poisson's ratio is less than 0.35 [18]. For this criterion Ni_{50-x}Ti₅₀Pt_x does not satisfy either component. However, the B19 phase is near this empirical range, and, since it also fulfills Pugh's criterion, it is more intrinsically ductile than the B2 structure.

Hardness is tied to the Young's modulus, and *ab initio* calculations for the NiTi B2 phase agree well with dynamically measured Young's moduli [13]: 90 GPa calculated versus 93-98 GPa experimental. Hardness decreases in this B2 system as Pt content is increased and is much higher for the B19 structure than for the B2 structure. Therefore, the elastic moduli indicate that the B19 structure is harder yet exhibits more signs of ductility than the B2 structure. This upholds the Muller-Achenbach-Seelecke model which states that the Young's modulus of the martensite must always be higher than its austenite counterpart, and explains elastic criteria governing the martensitic transformation.

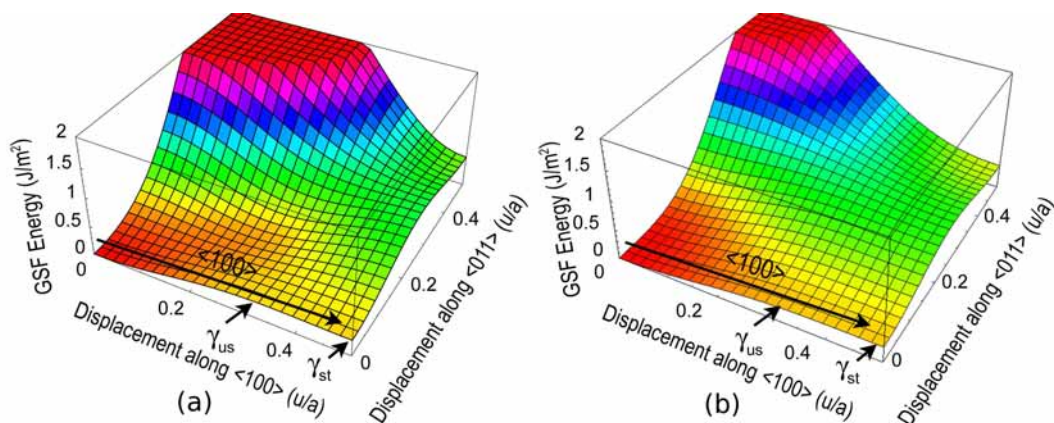


Fig. 4. 2 layer (a) NiTi and (b) NiTiPt GSF energy surfaces (relaxed).

To investigate properties such as ductility, crack blunting, and dislocation mobility, we perform generalized stacking fault (GSF) calculations throughout the (001), (011), and (111) shear planes to the unstable stacking fault in each direction. This was recently performed on equiatomic NiTi [5], and those results are compared with NiTi with Pt additions in the system in Table 2. We calculate this for various atomic layer thicknesses to determine the minimum number of layers to reduce surface coupling effects. Additionally, smaller layer thicknesses are examined to determine susceptibility to atomic shuffling as well as for insights into the atomistic transformation path.

GSF energy barriers for (001) shear were lower for Pt alloyed NiTi than for the equiatomic case. This is likely due to the larger lattice constant of the system which in turn allows atoms to move more freely. Similar results were obtained for (011) shear. However, the topology of the GSF surface changes, and while the energy barrier is lower at the unstable stacking fault, there is an additional barrier along the Burger's vector before that point (see Fig. 4). Even with this change in topology, the energy barriers are slightly lower than NiTi energy barriers for each thickness except the three layer thickness. Relaxation was applied to the two layer systems and reveals very low energy barriers for (011) shear (see Fig. 4). Given these low barriers and previous findings regarding the transformation path of equiatomic NiTi [10], the atomistic transformation mechanism for NiTiPt is likely involves $\langle 100 \rangle (011)$ shear occurring in bilayer pattern. The (111) GSF surface for equiatomic NiTi exhibited very high energy barriers and atomic overlaps prohibited calculations to the unstable stacking fault. Similar behavior was observed for NiTiPt in the (111) shear plane. Thus, Pt slightly lowers the energy barriers for (001) and (011) shear and changes the topology of (011) shear. The decrease in energy barriers should result in improved ductility in this system. A near instability is observed for $\langle 100 \rangle (011)$ 2 layer shear similar to the atomic shuffling mechanism of the NiTi martensitic transformation path [10].

As recently noted by Ref [11], the bonding character of NiTi changes as Pt is introduced into the system, breaking the hybridization of the Ni-Ti bonding in the B2 structure. We studied the densities of states of various concentrations Pt in NiTiPt and confirm this behavior as the lower energy d -states of platinum break the hybridization of NiTi d -states. This likely creates the additional instability to B19 formation and an unstable C' and low (011) shear barriers.

2.2 Conclusions

Although ternary metallic alloys present numerous challenges and complexities for computational materials design, we have shown that properties from the electronic structure to macroscopic observables may be accurately calculated from fully first-principles methods. Here, site preferences of the Pt atoms, structural parameters and formation energies, elastic moduli, and GSF energy surfaces were obtained. We have determined that Pt prefers Ni sites at the 3rd

NN, and that the austenite is around 4.5-6 kJ/mol*atom higher in energy than the martensite regardless of the Pt concentration.

The elastic properties of this alloy are examined, and we find that an unstable C' and increased C_{44} encourages B19 formation as Pt increases in NiTiPt instead of B19' formation in NiTi. Additionally, the B2 structure of NiTiPt is not as intrinsically ductile as its B19 structure martensite, although these empirical criteria warrant continued examination. The Muller-Achenbach-Seelecke model is confirmed for this system as the Young's modulus of the martensite is greater than that of the austenite. Topological changes in the GSF energetics and changes in their energy barriers occur due to Pt additions: (011) and (001) energy barriers are lowered and a likely transformation path which originates with $\langle 100 \rangle (011)$ bilayer shear remains from the binary structure. Finally, this behavior is traced to a change in the bonding between NiTi which is reduced by the addition of Pt atoms. As the hybridization is broken in these bonds, the resistance to a structural phase transformation is lowered and the unique shape memory behavior of the system is realized.

Acknowledgment

This work was supported by the AFOSR (grant number FA9550-07-1-0174), the ONR (grant number N00014-05-C-0241), and the NASA Graduate Student Researchers Program. Computer time was provided by DOD HPC centers NAVO, ARSC, ASC, and MHPCC under grants AFOSR15573FR1 and ONRDC07319050. The authors wish to thank Ron Noebe, Shipeng Qui, Raj Vaidyanathan, Libor Kovarik, and Michael Mills for fruitful discussions and for granting use of their experimental results before publication.

References

1. R. Noebe, Private communication (2009), NASA GRC.
2. E. Wimmer, H. Krakauer, M. Weinert, A. J. Freeman, Phys. Rev. B **24**(2), (1981) 864
3. J. P. Perdew, K. Burke, M. Ernzerhof, Phys. Rev. Lett. **77**, (1996) 3865
4. M. Weinert, G. Schneider, R. Podlucky, J. Redinger, J. Phys. Condens. Matter **21**, (2009) 084201
5. N. Hatcher, O. Y. Kontesevoi, A. J. Freeman, 'The role of elastic and shear stabilities in the martensitic transformation path of NiTi', Phys. Rev. B, (2009), submitted.
6. D. A. Papaconstantopoulos, G. N. Kamm, P. N. Pouloupoulos, Solid State Comm. **41**(1), (1982) 93
7. X. Huang, G. Ackland, K. Rabe, Nature Materials **2**, (2003) 307
8. C. Gong, Y. Li, Y. Yang, D. Yang, Modelling Simul. Mater. Sci. Eng. **14**, (2006) 33
9. M.-X. Wagner, W. Windl, Acta Mater. **56**, (2008) 6232
10. N. Hatcher, O. Y. Kontesevoi, A. J. Freeman, Phys. Rev. B **79**, (2009) 020202
11. C. Tan, X. H. Tian, G. Ji, T. L. Gui, W. Cai, Solid State Comm. (147), (2008) 8
12. Q. Hu, R. Yang, J. Lu, B. Wang, Johansson, L. Vitos, Phys Rev B **76**, (2007) 224201
13. S. Qui, R. Vaidyanathan, Private communication (2009), University of Central Florida.
14. R. Hill, Proc. Phys. Soc. London **65**, (1952) 349
15. W. Voigt, *Lehrbuch der Kristallphysik*. (Leipzig, Berlin 1910)
16. A. Reuss, Z Angew Math Mech **9**, (1929) 55
17. S. Pugh, Philos. Mag. **45**(367), (1954) 823
18. K. Gschneidner, et al., Nature Materials **2**, (2003) 587